

NASA TECHNICAL NOTE



NASA TN D-4559

NASA TN D-4559

e.1

LOAN COPY - RETURN
APR 1968
KENTLAND, OHIO

0131216



TECH LIBRARY KAFB, NM

SOME NUMERICAL COMPARISONS OF THREE-BODY TRAJECTORIES WITH PATCHED TWO-BODY TRAJECTORIES FOR LOW THRUST ROCKETS

by William C. Strack
Lewis Research Center
Cleveland, Ohio

TECH LIBRARY KAFB, NM



0131216

SOME NUMERICAL COMPARISONS OF THREE-BODY TRAJECTORIES WITH
PATCHED TWO-BODY TRAJECTORIES FOR LOW THRUST ROCKETS

By William C. Strack

Lewis Research Center
Cleveland, Ohio

NATIONAL AERONAUTICS AND SPACE ADMINISTRATION

For sale by the Clearinghouse for Federal Scientific and Technical Information
Springfield, Virginia 22151 - CFSTI price \$3.00

ABSTRACT

The n-body problem for low-thrust vehicles with optimal thrust control is formulated for the case of constant thrust with coast. A successive two-body approximation to the n-body problem is also developed under the assumption of tangential thrust during the planetocentric leg. This approximation involves one arbitrary parameter - the planetocentric radius at the patch point - whose best value can be determined by comparison with n-body solutions. Numerical solutions of several three-body problems indicate that the patch radius should be about 300 Earth radii for either a circular or a parabolic initial Earth orbit.

SOME NUMERICAL COMPARISONS OF THREE-BODY TRAJECTORIES WITH PATCHED TWO-BODY TRAJECTORIES FOR LOW THRUST ROCKETS

by William C. Strack
Lewis Research Center

SUMMARY

The n-body problem for low-thrust vehicles with optimal thrust control is formulated for the case of constant thrust with coast. Numerically calculated solutions are then presented for several transfers between an initial low-Earth orbit (circular or parabolic) and the orbit of Mars. A successive two-body approximation to the n-body problem is developed under the assumption of tangential thrust during the planetocentric leg. This approximation involves one arbitrary parameter - the planetocentric radius at the patch point - the best value of which can be determined by comparison with the n-body solutions. This value is found to be about 300 Earth radii for the circular initial Earth orbit case and for three different parabolic initial Earth orbit cases. If zero thrust is assumed for the planetocentric leg in the parabolic orbit case, the best value of the patch radius is between 100 and 160 Earth radii.

INTRODUCTION

The prospect of using low acceleration propulsion devices in interplanetary vehicles has led to the development of elaborate mathematical techniques (e. g. , calculus of variations schemes) that are used to optimize the thrust program along vehicle trajectories. These analyses are customarily carried out under the assumption of two-body motion and have proved quite useful in the solution of two broad classes of problems involving (1) two bodies only and (2) more than two bodies. The usual case involves a transfer from Earth to another planet. When the planetocentric legs of the trajectory are to be performed with high-thrust systems they are often ignored. The simplified problem then involves motion in a single gravitational field. The usual assumption is that low thrust commences in heliocentric space with a certain hyperbolic velocity (often zero) added to Earth's orbital velocity to determine the initial heliocentric velocity. The time required to escape from

Earth orbit is usually neglected and the initial heliocentric radius vector is assumed to be that of the Earth.

If the planetocentric maneuvers are performed with low-thrust systems a patching technique is ordinarily used wherein only two-body motion is assumed at any given time. Quite often tangential thrust spirals to escape energy are calculated with approximate analytical expressions. If the vehicle's planetocentric patch radius and velocity are assumed to be negligible in comparison to the Earth's heliocentric radius and velocity, then only the escape time and the propellant consumption during escape are needed to completely determine the heliocentric conditions at the patch point. The same approach is often used when the rocket is assumed to be on a parabolic coast path while in planetocentric space.

Several schemes following an approach commonly used in high-thrust trajectory studies have appeared recently (refs. 1 and 2) that introduce more realism into the models by relating the initial heliocentric conditions to both: (1) the planet's position and velocity and (2) the terminal planetocentric radius and velocity of the rocket. The switch from planetocentric to heliocentric coordinates takes place at a particular planetocentric radius called the patch radius in this report. The initial heliocentric conditions (mass, time, radius, and velocity) are then dependent upon the patch radius, the planetocentric thrust mode, and the size and shape of the initial planetocentric orbit. The planetocentric escape path can be determined either by precise numerical calculations or by approximate analytical expressions. In either case, the right patch radius and the proper spot on the patching sphere must be determined. The latter is easily taken care of by the transversality condition of the calculus of variations. The "right" patch radius is not so easily determined since the radius used in high-thrust studies is not necessarily applicable. If it is picked "properly," the approximate two-body calculation will yield the same mass ratio as the n-body calculation. The corresponding trajectories, however, will always differ slightly.

To date, no results have been presented comparing these approximate patching schemes with n-body variational solutions because the n-body solutions are difficult to obtain and require a large expenditure of computer time. The purpose of this report is to (1) present several three-body solutions and (2) compare the approximate two-body patching technique results with these more exact solutions.

Three-body solutions are generated for low thrust transfers from low Earth orbits to the mean heliocentric orbit of Mars. These solutions are for a simple problem model involving three bodies: the rocket, Sun, and Earth. This simplification in the sample problems allows attention to be focused on the main issue - trajectories that pass from one dominant gravitational field into another. The thrust vector is optimally directed and of constant magnitude. Coast phases are permitted. Two cases are considered: (1) initial circular orbit about Earth and (2) initial parabolic orbit about Earth. These cases

correspond to escapes utilizing (1) all low-thrust and (2) high thrust followed by low thrust. The corresponding patched two-body calculations are carried out under the same rules except that (1) tangential thrust is assumed for the Earth-centered portion of the trajectory and (2) the two-body assumption is imposed. The tangential thrust assumption is not critical since tangential thrust is very nearly optimum for low-thrust Earth escapes (ref. 3). Some solutions are also presented for the parabolic orbit case under the assumption that the vehicle coasts to the patching point.

ANALYSIS

The problem posed is: Given the initial state of a rocket in Earth orbit and a heliocentric final state, determine the low-thrust transfer trajectory that minimizes the propellant consumption. The accurate solution of such a problem is difficult and quite time consuming, and no results have appeared in the literature. A second question, therefore, arises: How can the actual solutions be closely approximated? This question will be discussed later.

N-Body Solutions

Statement of problem. - The rocket is assumed to operate with constant exhaust velocity engines that may be freely turned on or off. Furthermore, the thrust magnitude remains constant when the engines are operating. The vector equation of motion of such a rocket in a central force field perturbed by $n-2$ other bodies is:

$$\ddot{\mathbf{R}} = -\frac{\mu}{r^3} \mathbf{R} - \frac{c\dot{m}}{m} \mathbf{T} - \sum_{j=2}^{n-1} \mu_j \left(\frac{\mathbf{R} - \mathbf{R}_j}{|\mathbf{R} - \mathbf{R}_j|^3} + \frac{\mathbf{R}_j}{r_j^3} \right), \quad n \geq 3 \quad (1)$$

Figure 1 displays the geometry of the problem and all symbols are defined in appendix A. The center of the dominant gravitational body defines the origin of the coordinate system and the summation term vanishes for two-body motion.

The necessary conditions for minimizing the propellant consumption are given by the Euler-Lagrange equations (ref. 4):

$$\ddot{\lambda} = - \sum_{j=1}^{n-1} \frac{\mu_j}{r_j^3} \left[\lambda - \frac{3}{r_j^2} (\lambda \cdot R_j) R_j \right] \quad (2)$$

$$T = \frac{\lambda}{|\lambda|} \quad (3)$$

$$\dot{\sigma} = - \frac{c \dot{m}}{m^2} |\lambda| \quad (4)$$

where λ is the Lagrange multiplier vector (also called the adjoint variable or primer vector). R_1 , r_1 , and μ_1 in equation (2) are identical to R , r , and μ in equation (1). The choice of on or off mode of engine operation is determined by:

$$\dot{m} = 0 \quad \text{if } [c|\lambda| - \sigma m < 0] \quad (5)$$

$$\dot{m} = \dot{m}_{\max} \quad \text{if } [c|\lambda| - \sigma m > 0] \quad (6)$$

Equations (1) to (6) comprise a set of second order nonlinear differential equations that must be numerically integrated to yield solutions. Equations (1) and (2) are equivalent to the following first order set of differential equations:

$$\dot{V} = - \frac{\mu}{r^3} R - \frac{c \dot{m}}{m} \frac{\lambda}{|\lambda|} - \sum_{j=2}^{n-1} \mu_j \left(\frac{R - R_j}{|R - R_j|^3} + \frac{R_j}{r_j^3} \right) \quad (7)$$

$$\dot{R} = V \quad (8)$$

$$\lambda = -\dot{\lambda} \quad (9)$$

$$\dot{\lambda} = \sum_{j=1}^{n-1} \frac{\mu_j}{r_j^3} \left[\lambda - \frac{3}{r_j^2} (\lambda \cdot R_j) R_j \right] \quad (10)$$

Just as in the case of two-body motion, the transversality condition (ref. 4) is:

$$-dm_f + [\lambda \cdot dV + \lambda \cdot dR + \sigma dm - C dt]_0^f = 0 \quad (11)$$

where 0 and f denote values taken at the beginning and end of the optimal control phase, respectively. This equation imposes boundary conditions in addition to those explicitly required in the problem definition. On a solution trajectory a differential vanishes at either end point in equation (11) if its corresponding variable has a specified value at that terminus, otherwise the differential is nonzero and its coefficient must vanish. In particular, since m_f is not specified, equation (11) shows that $\sigma_f = 1$. C is a constant of the motion and is given by

$$C = \lambda \cdot \dot{V} + \lambda \cdot \dot{R} + \sigma \dot{m} = \text{constant} \quad (12)$$

The following additional vector constant of the motion is valid for the two-body problem only (ref. 5):

$$\lambda \times \dot{R} + R \times \dot{\lambda} = \text{a vector constant} \quad (13)$$

Two types of discontinuities may occur along a trajectory. First, \dot{m} may switch from \dot{m}_{\max} to zero or vice-versa. The Weierstrass-Erdmann corner condition (ref. 4) stipulates that λ , λ , and σ are continuous across such corners and it is easy to show that C is also continuous at such points. Second, in the case of n-bodies, a coordinate system change may take place at a certain planetocentric radius. Thus, R and V are subject to discontinuities. At the translation point C is also discontinuous.

Boundary value problem. - The boundary conditions at the initial and final points are satisfied by successive iterations of the initial values of λ and λ . In practice, the initial value of σ may be arbitrarily chosen since the set of equations (4) to (10) is homogeneous and the $\sigma_f = 1$ condition may be satisfied simply by rescaling the multipliers after the boundary-value problem is solved. Many iterative techniques may be used to satisfy the terminal boundary conditions. The technique employed in this study is a hybrid combination consisting of (1) successive univariate searches when the error function is relatively large and (2) a multivariate Newton-Raphson scheme when the error function is relatively small. The error function is simply a weighted summation of the squared differences between the final desired and current boundary conditions. Rather than computing the required partial derivatives of the Newton-Raphson scheme by finite differencing, the partial derivatives were generated by integrating an additional set of equations simultaneously with each trajectory calculation. The advantages of this technique are that convergence of the Newton-Raphson scheme is facilitated since the resultant partial derivatives are more accurate, decisions about the increments in the initial values of λ

and λ used for the perturbation trajectories are avoided, and less computer time is required for a solution. For example, inclusion of a third body in the problem makes solutions very difficult to obtain by a finite difference scheme but relatively easy with analytical partial derivative generation. These additional differential equations come directly from the equations of motion and the Euler-Lagrange equations. Differentiating equations (4) to (10) with respect to an arbitrary variable γ_i and inverting the order of differentiation, after simplifying, yields:

$$\frac{d}{dt} \left(\frac{\partial V}{\partial \gamma_i} \right) = - \sum_{j=1}^{n-1} \frac{\mu_j}{r_j^3} \left[\frac{\partial R}{\partial \gamma_i} - \frac{3}{r_j^2} \left(\mathbf{R}_j \cdot \frac{\partial \mathbf{R}}{\partial \gamma_i} \right) \mathbf{R}_j \right] + c \frac{\dot{m}}{m} \frac{\lambda}{|\lambda|} \left[\frac{1}{m} \frac{\partial m}{\partial \gamma_i} - \frac{1}{\dot{m}} \frac{\partial \dot{m}}{\partial \gamma_i} + \left(\frac{\lambda}{|\lambda|^2} \cdot \frac{\partial \lambda}{\partial \gamma_i} \right) - \frac{1}{\lambda} \frac{\partial \lambda}{\partial \gamma_i} \right] \quad (14)$$

$$\frac{d}{dt} \left(\frac{\partial R}{\partial \gamma_i} \right) = \frac{\partial V}{\partial \gamma_i} \quad (15)$$

$$\frac{d}{dt} \left(\frac{\partial \lambda}{\partial \gamma_i} \right) = - \frac{\partial \lambda}{\partial \gamma_i} \quad (16)$$

$$\frac{d}{dt} \left(\frac{\partial \lambda}{\partial \gamma_i} \right) = \sum_{j=1}^{n-1} \frac{\mu_j}{r_j^3} \left(\frac{\partial \lambda}{\partial \gamma_i} - \frac{3}{r_j^2} \left\{ \left(\mathbf{R}_j \cdot \frac{\partial \mathbf{R}}{\partial \gamma_i} \right) \lambda + (\lambda \cdot \mathbf{R}_j) \frac{\partial \mathbf{R}}{\partial \gamma_i} + \left[\frac{\partial(\lambda \cdot \mathbf{R}_j)}{\partial \gamma_i} - \frac{5}{r_j^2} (\lambda \cdot \mathbf{R}_j) \left(\mathbf{R}_j \cdot \frac{\partial \mathbf{R}}{\partial \gamma_i} \right) \right] \mathbf{R}_j \right\} \right) \quad (17)$$

$$\frac{d}{dt} \left(\frac{\partial \sigma}{\partial \gamma_i} \right) = \frac{2c\dot{m}|\lambda|}{m^3} \frac{\partial m}{\partial \gamma_i} - \frac{c|\lambda|}{m^2} \frac{\partial \dot{m}}{\partial \gamma_i} - \frac{c\dot{m}}{m^2|\lambda|} \left(\lambda \cdot \frac{\partial \lambda}{\partial \gamma_i} \right) \quad (18)$$

$$\frac{d}{dt} \left(\frac{\partial m}{\partial \gamma_i} \right) = \frac{\partial \dot{m}}{\partial \gamma_i} \quad (19)$$

when \dot{m} is constant, $\partial\dot{m}/\partial\gamma_i = 0$ and equation (19) reduces to the trivial identity $0 = 0$. With the assumption of constant thrust, \dot{m} is constant everywhere except the points at which $c|\lambda| - \sigma m = 0$ in which case $\partial\dot{m}/\partial\gamma_i$ is unbounded causing jump discontinuities in all equations containing a $\partial\dot{m}/\partial\gamma_i$ term. The appendix of reference 6 shows that the magnitude of these jumps is given in general by:

$$\Delta \left(\frac{\partial S_j}{\partial \gamma_i} \right) = \frac{\left(\dot{S}_j \right)_{\text{power off}} - \left(\dot{S}_j \right)_{\text{power on}}}{\dot{\mathcal{H}}} \frac{\partial \mathcal{H}}{\partial \gamma_i} \quad (20)$$

where

$$S_j \equiv V, \sigma, \text{ or } m$$

$$\mathcal{H} = \frac{c|\lambda|}{m} - \sigma \quad (21)$$

$$\dot{\mathcal{H}} = - \frac{c}{m|\lambda|} (\lambda \cdot \kappa) \quad (22)$$

$$\frac{\partial \mathcal{H}}{\partial \gamma_i} = \frac{c}{m|\lambda|} \left(\lambda \cdot \frac{\partial \lambda}{\partial \gamma_i} \right) - \frac{\partial \sigma}{\partial \gamma_i} - \frac{c|\lambda|}{m^2} \frac{\partial m}{\partial \gamma_i} \quad (23)$$

(a continuous function everywhere). Specifically,

$$\Delta \left(\frac{\partial V}{\partial \gamma_i} \right) = - \frac{\partial \mathcal{H}}{\partial \gamma_i} \frac{\dot{m}_{\max}}{(\lambda \cdot \kappa)} \lambda \quad (24)$$

$$\Delta \left(\frac{\partial \sigma}{\partial \gamma_i} \right) = - \frac{\partial \mathcal{H}}{\partial \gamma_i} \frac{\dot{m}_{\max} |\lambda|^2}{m(\lambda \cdot \kappa)} \quad (25)$$

$$\Delta \left(\frac{\partial m}{\partial \gamma_i} \right) = \frac{\partial \mathcal{H}}{\partial \gamma_i} \frac{\dot{m}_{\max} |\lambda|^2}{\sigma(\lambda \cdot \kappa)} \quad (26)$$

It should be noted that these partial derivatives are continuous under an origin translation. Also, the partial derivative equations (14) to (19) are insufficient by themselves

for the case of unspecified terminal time. Only fixed terminal time cases are considered here. When coast phases are permitted the γ_i are taken to be the initial values of λ and λ . When the problem does not allow coast phases, σ is superfluous and the initial value of any one of the components of λ or λ may be arbitrarily selected. For this case, one of the γ_i is taken to be \dot{m} since for fixed time problems \dot{m} is unique but unknown. The initial values of the partial derivatives are functions of the initial boundary conditions. For example, if the values of V_0 and R_0 are fixed then all partial derivatives are initially zero except $[\partial\lambda/\partial\lambda]_0$ and $[\partial\lambda/\partial\lambda]_0$ which are unit diagonal matrices. But if V_0 and R_0 are some function of λ_0 , then the initial values of $\partial V/\partial\gamma_i$ and $\partial R/\partial\gamma_i$ are not all zero. Adding a fixed amount of velocity via high thrust propulsion to some reference velocity (e. g. , the Earth's orbital velocity) in an optimal direction is an example in point. This will be made more explicit later.

The Newton-Raphson iteration scheme can be represented mathematically by:

$$\gamma_{\text{new}} = \gamma_{\text{old}} + k(\Delta\gamma) \quad (27)$$

$$\Delta\gamma = A^{-1}(\Delta B) \quad (28)$$

where k is a damping factor whose value lies between 0 and 1, ΔB is the vector of residual errors in the boundary conditions, and $[A]$ is the square matrix of partial derivatives $\partial B_i/\partial\gamma_j$. The elements of $[A]$ are composed of a subset of the definite integrals of equations (14) to (19) or combinations of these integrals depending upon the form of the end conditions. If the end conditions are given by (point to point problem):

$$V_f = \bar{V} \quad (29)$$

$$R_f = \bar{R} \quad (30)$$

where a bar denotes a desired value, then $[A]$ consists simply of the elements $(\partial V/\partial\gamma_i)_f$ and $(\partial R/\partial\gamma_i)_f$. For the flyby problem with fixed terminal distance but free velocity and path angle, the end conditions are:

$$r_f = \bar{r} \quad (31)$$

$$\lambda_f = 0 \quad (32)$$

and the elements of $[A]$ consist of $(\partial r / \partial \gamma_i)_f$ and $(\partial \lambda / \partial \gamma_i)_f$. Here $(\partial \lambda / \partial \gamma_i)_f$ is determined by integrating equation (16) and $(\partial r / \partial \gamma_i)_f$ is determined by integrating equation (15) via the relation

$$\frac{\partial r}{\partial \gamma_i} = \frac{1}{r} \left(R \cdot \frac{\partial R}{\partial \gamma_i} \right) \quad (33)$$

Obviously many other sets of end conditions are possible and each of these results in a different form for the elements of $[A]$.

Most of the results presented later are stated in terms of the propellant expenditure. In this connection, the final mass value may be linearly corrected for residual errors in the terminal boundary conditions. In the simplest case the terminal boundary conditions are fixed values of the state variables V and R . Since λ and λ may be interpreted (ref. 7) as the partial derivatives of the negative of the final mass with respect to their corresponding problem variables,

$$\bar{m}_f \cong m_f + \left[\lambda \cdot (V - \bar{V}) + \lambda \cdot (R - \bar{R}) \right]_f \quad (34)$$

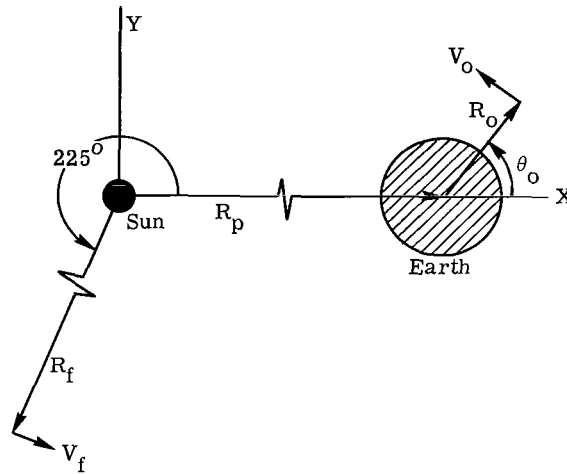
λ_f and λ_f are assumed to be normalized by $\sigma_f = 1$ as required by the transversality condition.

Procedure. - The specific problem for which numerical results are later presented is the following: At time zero the Earth is on the X-axis of a heliocentric coordinate system and a space vehicle is at the perigee of an orbit about Earth. The perigee altitude is 185 km and the vehicle's orbit about Earth is either circular or parabolic. At the specified final time the vehicle arrives at the orbit of Mars after traversing 225° (arbitrarily chosen) of total heliocentric angle. For simplicity, the orbits of Mars and Earth are assumed to be circular and coplanar with the vehicle's initial orbit about Earth. Table I contains a list of assumed values of problem constants and table II displays the combinations of trip time and initial thrust-weight ratio F/W picked for sample cases.

Sketch (a) shows the geometry. The angular location of the initial point with respect to the X-axis θ_0 is free to be optimized. The optimization can be accomplished by satisfying the transversality condition (eq. (11)) or, alternatively, by employing any sort of simple search scheme. Specifically, the transversality condition requires that

$$\left(\lambda_1 v \cos \theta + \lambda_2 v \sin \theta + \lambda_1 r \sin \theta - \lambda_2 r \cos \theta \right)_0 = 0 \quad (35)$$

where λ_1 and λ_2 are the X and Y components of λ and similarly for λ_1 , λ_2 , and λ .



(a)

The numerical calculations were carried out with the present version of the Lewis N-Body Code which uses a fourth order Runge-Kutta integration scheme with variable step size control (ref. 8). Test cases showed that solution values were quite insensitive to the planetocentric radius at which the origin was translated from the Earth to the Sun. Over the range of 25 to 10 000 Earth radii, the final mass change was less than two units in the sixth significant figures. The particular radius used for data generation was 145 Earth radii. Obtaining solutions for n-body problems is substantially more difficult than for two-body problems. The computer time alone is one to two orders of magnitude greater for n-body solutions compared to two-body solutions. The solution method used for this study is briefly summarized as follows: First, obtain the solution of a relatively simple problem that only approximates the actual problem. The simple problem is obtained by setting $\mu_2 = 0$ so that third body effects are ignored and by using a tangential thrust program until $r = r^*$ before switching to optimal thrusting. Second, gradually increase μ_2 to its real value by solving a series of problems with μ_2 as a parameter. Third, reduce r^* to the initial radius r_{in} through another series of problems. Finally, when $r = r_{in}$ the solution obtained is the actual n-body solution of the original problem. When one such solution has been obtained, the precise solution of other problems can be found by solving a series of problems starting in the neighborhood of the solved problem and proceeding toward the desired one. The only real difficulty with the above procedure is that as r^* approaches r_{in} the trajectories become increasingly more sensitive to changes in the initial values of λ and λ . This situation becomes so severe that convergence is impossible for r^* less than about 20 Earth radii due to the limited number of significant figures carried by the computer (8 in this study). Although distressing, this situation is not so bad as to prevent meaningful answers from being obtained. This is

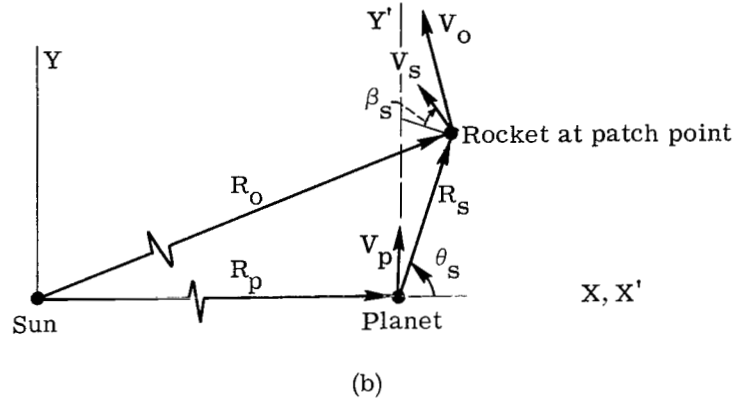
true because, as was stated in the INTRODUCTION, tangential thrust is very nearly optimum for small r , and therefore, a plot of m_f against r^* can be extrapolated to r_{in} quite accurately (i. e. , to 4 significant figures).

Approximate Patched Two-Body Solutions

Patched two-body approximations to the low-thrust n-body problem are popular because of their computational simplicity. The assumption usually made is that the rocket coasts or is tangentially propelled to the patching point ignoring the Sun's gravitational effect. From that point on the rocket motion is calculated under the influence of no other gravitational body except the Sun. The equations of motion are much simpler and can be solved analytically for coast phases. When low-thrust propulsion commences from a circular planetocentric orbit, tangential thrust is most often assumed because it is very nearly optimal (ref. 3) up to the escape condition. When the initial planetocentric orbit is parabolic or hyperbolic, coast flight is usually assumed for the planetocentric leg, although tangential thrust is also sometimes assumed. Furthermore, the tangentially powered motion in planetocentric space is almost always represented with one of many analytic methods (e. g. , refs. 11 and 12). Optimal thrust programming begins in heliocentric space.

In this study tangential thrust is assumed for the planetocentric leg and optimal thrust control is used for the heliocentric leg. Furthermore, the tangential thrust phase is numerically integrated rather than approximated in order to avoid results that are dependent upon specific approximations. In some cases the time optimal control policy calls for a coast phase at the end of the planetocentric leg. This situation can be detected by the presence of an initial coast phase on the heliocentric leg and in this case an iteration on the planetocentric coast duration is required to determine the best two-body patched trajectory.

As in the n-body problem, the initial heliocentric position and velocity of the vehicle are obtained by vectorially adding the vehicle's planetocentric position and velocity at the patching point to the heliocentric position and velocity of the departure planet. However, since the initial planetocentric point may be anywhere on a sphere of radius r_s , the patching point on this sphere is also arbitrary. This arbitrariness is removed by requiring that the patch point be the optimal one. This in turn determines the optimal planetocentric starting point. Suppose that in general the position of the departure planet is R_p relative to a Cartesian coordinate system with the origin located at the center of the Sun (see sketch (b)). Let the planet's velocity be V_p and let the vehicle position and velocity at the patch point relative to a planet centered coordinate system (alined with the



Sun centered system) be R_S and V_S . Then, relative to the Sun:

$$R_O = R_p + R_S \quad (36)$$

$$V_O = V_p + V_S \quad (37)$$

And from sketch (b), for the two-dimensional case, the components of R_S and V_S are

$$x' = r_S \cos \theta_S \quad (38)$$

$$y' = r_S \sin \theta_S \quad (39)$$

and

$$\dot{x}' = -v_S \sin (\theta_S - \beta_S) \quad (40)$$

$$\dot{y}' = v_S \cos (\theta_S - \beta_S) \quad (41)$$

The transversality condition (eq. (11)) requires that

$$\lambda_O \cdot dV_O + \lambda_O \cdot dR_O = 0 \quad (42)$$

Evaluating this expression with the aid of equations (36) to (41) and noting that R_p , V_p , r_S , v_S , and β_S are all fixed, and solving for the optimum value of θ_S yields

$$\tan \theta_s = \frac{v_s(-\lambda_1 \cos \beta_s + \lambda_2 \sin \beta_s) + \lambda_2 r_s}{v_s(\lambda_1 \sin \beta_s + \lambda_2 \cos \beta_s) + \lambda_1 r_s} \equiv \frac{D}{E} \quad (43)$$

so,

$$\cos \theta_s = \frac{E}{\pm \sqrt{D^2 + E^2}} \quad \sin \theta_s = \frac{D}{\pm \sqrt{D^2 + E^2}} \quad (44)$$

Convincing arguments that the plus sign is correct in equation (44) are given in reference 2. Similar relations for the three dimensional case exist but are quite lengthy (two additional degrees of freedom are involved). As stated earlier, problems that have an initial optimal control point that is not fixed but lies on some curve or surface cause some of the analytical partial derivatives to have initial values dependent on the boundary surface function. The heliocentric leg of the two-body patched scheme outlined above is a case in point. From equations (36) and (37),

$$\left(\frac{\partial \mathbf{R}}{\partial \gamma_i} \right)_0 = \frac{\partial \mathbf{R}_s}{\partial \gamma_i} \quad (45)$$

$$\left(\frac{\partial \mathbf{V}}{\partial \gamma_i} \right)_0 = \frac{\partial \mathbf{V}_s}{\partial \gamma_i} \quad (46)$$

These equations are solved for the cases $\gamma_i = \lambda_{i,0}$ and $\gamma_i = \lambda_{i,0}$ in appendix B.

This completes the analysis of the n-body and patched two-body techniques used in this report. The remaining portion is devoted to several specific examples that compare three-body solutions with patched two-body solutions.

RESULTS AND DISCUSSION

Three-Body Solutions

The sample problems all involve a transfer from an Earth orbit condition to the orbit of Mars. The main concern here is the computation of optimal thrust trajectories that essentially leave one gravitational field and enter another. All unnecessary complicating aspects of a real problem are avoided. Thus, the n-body problem is reduced to

a three-body problem by ignoring the minor perturbative effects of bodies other than the Sun and the Earth. Furthermore, the orbits of Earth and Mars are taken to be circular and coplanar with the vehicle's orbit. Three dimensional ephemeris data and additional bodies can just as well be included (i. e., the computer code used contains such realism) but would serve no useful purpose here.

The trajectories for case 1 and 2 of table II are diagrammed in figures 2 to 4. These cases are for 275-day/225° transfers with $F/W = 10^{-4}$. Figure 2 shows the planetocentric phase for the case of an initial parabolic orbit about Earth. As explained in the ANALYSIS section, a short tangential thrust phase is necessary at the start of the trajectory for computational convenience. The switch from tangential to optimal thrust control takes place at 23 Earth radii. In Earth space the optimal angle-of-attack (angle from the velocity vector to the thrust vector) increases from 0.5° at the initial point to only 5.2° at the origin translation point. Thus, it is quite unlikely that replacing the short tangential thrust phase with optimal control would cause any significant change in either the trajectory or the optimal angle-of-attack schedule.

Figure 3 shows the planetocentric phase for an initial circular orbit about Earth. Only the last two turns of the spiral are shown and the optimal control policy begins at 20 Earth radii. The angle-of-attack history is again nearly tangential but oscillates, starting at +4°, dipping to -13°, and then rising to -2.5° at the origin translation point. This behavior has been noted before in the optimal Earth escape problem (ref. 3). It consists of minute oscillations of the thrust vector about the velocity vector until the last few turns of the spiral where the amplitude of the oscillation grows quite rapidly.

The heliocentric portions of cases 1 and 2 are displayed in figure 4. Both trajectories are rather typical, having a mixture of power and coast phases. The parabolic orbit case has two coast phases but the circular orbit case has only one. The entire angle-of-attack histories are shown in figure 5 for both cases. The initial tangential thrust portion for the parabolic orbit case is so short that it is not detectable in the scale of this figure. Quite the reverse is true for the circular orbit case. Here the tangential thrust portion is seen to last about 67 days and represents the average angle-of-attack history of the true oscillatory solution. The optimal thrust angle history in inertial space is, of course, continuous across the origin translation. However, the discontinuity in the velocity vector at this point causes a discontinuity in the angle-of-attack history as seen in this figure.

Mentioned earlier was the fact that a one-parameter sequence of solutions is obtained wherein the parameter is the radius of the switch point from tangential to optimal thrust control. Ideally, this sequence is terminated when the switching radius becomes equal to the initial radius thus eliminating the tangential thrust phase. Practically, numerical difficulties prevent solutions from being obtained when the switching radius falls below about 20 Earth radii. Nonetheless, such a terminated sequence allows the ideal solution to be accurately determined to more than four significant figures in the propellant expenditure

by extrapolation. Having determined the three-body solution (see table II for propellant fractions), the percent increase in propellant expenditure is plotted against the switching radius r^* in figure 6. The two curves in figure 6 have discontinuous slopes at the origin translation radius because the tangential thrust vector is discontinuous there (i. e. , tangential thrust with respect to the Sun is different than tangential thrust with respect to Earth). This effect is much more pronounced in the parabolic orbit case because the initial optimal control in heliocentric space is much farther from tangential than in the circular orbit case (see fig. 5). In either case figure 6 suggests that if the rocket is in heliocentric space and not too far from the planet then tangential thrust with respect to the planetocentric velocity vector is better than tangential thrust with respect to the heliocentric velocity vector. The most important point though is that tangential thrusting in planetocentric space is not far from optimal in terms of propellant expenditure. That is, instead of insisting that $r^* = r_{in}$, r^* may be as large as 145 Earth radii with less than a 0.12 percent penalty for the circular orbit case and less than 0.01 percent penalty for the parabolic orbit case. The much smaller penalty for the parabolic orbit case is a result of the much smaller time period associated with these nonoptimal phases (e. g. , 1/2 day against 67 days for $r^* = 25$ Earth radii).

Cases 1 and 2 illustrate the essential features of the three-body solutions. Cases 3 and 4 are presented mainly to show what effect changes in F/W and mission ΔV have on the comparison between three-body and patched two-body solutions. These comparisons are given in the next section.

Patched Two-Body Solutions

Most of the patched two-body solutions used to approximate the three-body solutions consist of a tangentially propelled planetocentric leg followed by a heliocentric leg with optimal thrust control. Some results are also given for planetocentric coasting (instead of tangential thrusting) for the parabolic orbit case. In all cases the decision must be made of when to terminate the planetocentric leg and commence the heliocentric leg. The patch point is chosen to occur at a specified planetocentric radius r_s . This patch radius may, in fact, be so chosen that the correct propellant expenditure is calculated (i. e. , the propellant expenditure agrees with the three-body solution). Of course, the two-body and three-body trajectories will differ slightly, but that is not critical for most mission analysis studies.

The fact that a correct patch radius exists is easy to see by examining the two limiting cases $r_s = r_{in}$ and $r_s = \infty$. If $r_s = r_{in}$ the Earth's gravitational field is lost and, therefore, (1) the propellant needed to escape the Earth is saved and (2) the propellant needed for the heliocentric leg is reduced. The heliocentric propellant is reduced

for two reasons. First, the initial heliocentric velocity will be most favorable since V_s increases as r_s decreases. Second, the heliocentric travel angle and time will be a maximum thus allowing the most efficient trajectory. These effects taken together cause the required ΔV to be minimal. Thus, the two-body propellant mass is less than the three-body propellant mass if r_s is sufficiently small.* On the other hand, as $r_s \rightarrow \infty$ the propellant mass increases until it approaches the initial mass or the planetocentric time exceeds the total mission time. Clearly then, the two-body propellant mass exceeds the three-body propellant mass if r_s is sufficiently large.

Tangential thrust for planetocentric leg. - The ratio of the two-body propellant mass to the three-body propellant mass is presented in figure 7 for cases 1 to 4 with tangential thrusting to r_s . The tangential portion is calculated exactly to determine the correct time, velocity, and path angle at r_s . Equations (36) to (44) are then employed to determine the optimum initial heliocentric position and velocity. Finally, equations (4) to (10) are integrated to determine the optimal heliocentric trajectory. The ratio of propellant masses increases as r_s increases in accordance with the reasons given in the previous paragraph. Figure 7 shows that at $r_s = 300$ Earth radii the ratio is nearly unity for every case. This indicates that $r_s \approx 300$ Earth radii is the correct value for the two-body patch radius. For $r_s < 300$ Earth radii not enough propellant is calculated by the two-body approximation and for $r_s > 300$ Earth radii too much propellant is calculated. Note also that for $r_s > 150$ Earth radii the curves are fairly flat and the maximum propellant error in the two-body scheme for $150 < r_s < 600$ Earth radii is about 3 percent. Larger errors prevail at $r_s < 150$ Earth radii.

The case of an initial circular orbit about the Earth is the least sensitive of all cases investigated. r_s values between 250 and 600 Earth radii give rise to less than 1/2 percent error in this particular case. Sometimes the patching radius for two-body schemes involving an escape spiral is taken to be that radius at which escape energy is attained. This radius is problem dependent and varies considerably with acceleration level. For the case considered here, escape occurs at 80 Earth radii and this gives rise to a -3 percent propellant error as noted on figure 7. The other three cases are all for an initial parabolic Earth orbit. Reducing the F/W from 10^{-4} to 0.56×10^{-4} reduces the correct r_s from 310 to 285 Earth radii and increases the sensitivity of the error to r_s by about 30 percent. Reducing the trip time from 275 days to 240 days (this increases the mission ΔV requirement by a factor of $2\frac{1}{2}$) causes no change in the correct value of r_s and only slightly decreases the sensitivity of the error to r_s .

Coast for planetocentric leg. - If the initial planetocentric orbit is parabolic no thrust

*In the extreme cases of very small mission ΔV and/or high F/W , the heliocentric powered phases can disappear entirely as r_s is reduced. In such a case the minimum propellant case occurs at $r_s > r_{in}$.

is needed to reach the patching point. The vehicle may be allowed just to coast to this point. Assuming coast flight for the planetocentric leg instead of tangential thrust for the parabolic initial orbit case leads to the results given on figure 8. The dot-dash curve is for the additional assumption $V_s = 0$ and illustrates that this assumption causes the two-body approximation to be over 10 percent conservative for this particular problem. The other two curves show that the coast assumption alone increases the sensitivity of the error to r_s and also reduces the correct value of r_s from about 300 Earth radii to 100 to 160 Earth radii depending upon F/W . This marked increase in sensitivity and range of "correct r_s " is not surprising in view of the significant coast durations involved (e. g. , 23 days for $r = 300$ Earth radii). The tangential thrust assumption is definitely preferable to the coast assumption with respect to the sensitivity and range considerations. The trajectories will also be more accurate under the tangential thrust assumption since this mode of operation more closely approximates the three-body solution.

Comparison of r_s to analytic sphere of influence radius. - The classical sphere of influence radius is obtained by setting the ratio of the perturbative force to primary force in planetocentric coordinates equal to the same ratio in heliocentric coordinates (ref. 9). This gives rise to a value of 145 Earth radii for the Earth-Sun system. This value is roughly in agreement with the planetocentric coast results ($100 < r_s < 160$ Earth radii) found in this study. But it is only 1/2 the value found under the tangential thrust assumption.

Another sphere of influence definition (ref. 10) sets the Sun's perturbative force equal to the planetocentric force, computed in planetocentric coordinates. The formula (derived in ref. 10) for r_s using this definition is:

$$r_s = (\text{planet's orbit radius}) \left(\frac{1}{2} \frac{\text{Planet mass}}{\text{Sun mass}} \right)^{1/3} \quad (47)$$

This leads to a sphere of influence radius of 270 Earth radii for the Earth-Sun system. This value compares quite well with the empirical values ($280 < r_s < 320$ Earth radii) found here under the tangential thrust assumption. Extending the usefulness of equation (47) to other planet-Sun systems is tempting because of the good correlation in the Earth-Sun case, but such an extension must be regarded as quite speculative at the present time.

The natural suggestion based on the limited number of cases investigated is to employ tangential thrust for the Earth-centered leg (since it agrees with the three-body power mode) and to use 300 Earth radii for the two-body patching radius r_s .

CONCLUDING REMARKS

The three-body variational solutions obtained provide reference data useful in the evaluation of approximation schemes. The optimal thrust direction in planetocentric space is nearly tangential and this leads to the assumption of tangential thrust during the planetocentric leg of the patched two-body scheme. Under this assumption, a value of 300 Earth radii for the patch radius never causes more than 1/2 percent error in propellant consumption for each of the four cases. Of course, these four cases do not cover a wide enough range of problems to conclude that 300 Earth radii is a good value for most problems. Nonetheless, the fact that doubling the F/W , doubling the mission ΔV , or changing the initial Earth orbit from circular to parabolic causes such small disturbances in the error at this value leads one to believe that it may hold over a much greater range of problems than considered here. Other destinations, for instance, would probably not affect the Earth-centered leg significantly so that this type of problem alternation is unlikely to affect the answers found here. If a nontangential thrust program were specified because of a system constraint (such as for solar-electric propulsion system), the results found here again would seem to be applicable.

The planetocentric coast assumption produces less uniformity in the correct value of r_s and significantly increases the propellant error at other r_s . It also decreases the correct value of r_s to 100 to 160 Earth radii. Only parabolic initial Earth orbit cases are examined here although the circular orbit case can also be done if the coast phase begins after escape energy is attained. In either case, a planetocentric coast phase assumption simplifies the problem (permits closed form solutions to the planetocentric trajectory) at the expense of accuracy. It should be noted here that if the three-body trajectories have a relatively large planetocentric coast arc, instead of a thrusting arc, the right value of r_s may well be about 300 Earth radii instead of 100 to 160 Earth radii. This conjecture is unresolved at the present time.

It seems that the most accurate method of approximating the three-body solution is to numerically calculate both a powered planetocentric leg and a heliocentric leg. It is quite possible that the need to numerically calculate the planetocentric leg can be removed through the use of analytic approximations such as are found in references 11 and 12. This would certainly reduce the required computer time necessary to obtain solutions but still retain a high degree of accuracy.

Lewis Research Center,
National Aeronautics and Space Administration,
Cleveland, Ohio, January 24, 1968,
789-30-01-01-22.

APPENDIX A

SYMBOLS

A	partial derivative matrix	ΔV	characteristic velocity increment, m/s
B	residual error vector		
C	first integral of Euler-Lagrange equation	V_p	velocity vector of a planet relative to the Sun, m
c	rocket exhaust velocity, m/s	V_s	velocity vector of the rocket at the patching point, m/s
D	defined by equation (43)	v, v_s	magnitude of V and V_s , respectively, m/s
E	defined by equation (43)		
F/W	initial thrust-weight ratio	X, Y	coordinate axes, origin at Sun center
\mathcal{H}	switching function defined by equation (21)	X', Y'	coordinate axes, origin at planet center
k	damping factor	x', y'	X', Y' components of R_s , m
m	mass of rocket, kg	β	path angle
R	position vector of rocket, m	γ	vector of unknown initial condition variables, usually composed of λ_0 and λ_0
R_j	vector from j^{th} gravitational body to rocket, m	θ	central angle of rocket relative to the X-axis
R_p	position vector of a planet relative to the Sun, m	λ	Lagrange multiplier vector associated with velocity
R_s	planetocentric position vector at which the two-body patching scheme is effected, m	λ	Lagrange multiplier vector associated with position
r^*	radius at which optimal thrust control begins, m	$ \lambda $	magnitude of vector λ (λ is any vector)
r, r_j, r_s	magnitude of R, R_j , and R_s , respectively, m	μ_j	gravitational constant of j^{th} gravitational body, m^3/s^2
S_j	V, σ , or m	σ	Lagrange multiplier associated with mass
T	unit vector in thrust direction		
V	rocket velocity vector, m/s		

Subscripts:

f end of optimal control
i the i^{th} component of a vector
in start of complete trajectory
j the j^{th} gravitational body
max maximum

o start of optimal control

s at the patching point

Superscripts:

- desired value

· differentiation with respect to
 time

APPENDIX B

INITIAL VALUES OF THE ANALYTICAL PARTIAL DERIVATIVES

Derived here are the initial values of the analytical partial derivatives for the two-dimensional heliocentric leg of the two-body patched scheme. From equations (38) to (41), (45) and (46) the required derivatives have the initial values:

$$\left(\frac{\partial \dot{\mathbf{x}}'}{\partial \gamma_{\mathbf{i}}}\right)_0 = -r_{\mathbf{s}} \sin \theta_{\mathbf{s}} \left(\frac{\partial \theta_{\mathbf{s}}}{\partial \gamma_{\mathbf{i}}}\right)_0 \quad (48)$$

$$\left(\frac{\partial \dot{\mathbf{y}}'}{\partial \gamma_{\mathbf{i}}}\right)_0 = r_{\mathbf{s}} \cos \theta_{\mathbf{s}} \left(\frac{\partial \theta_{\mathbf{s}}}{\partial \gamma_{\mathbf{i}}}\right)_0 \quad (49)$$

$$\left(\frac{\partial \dot{\mathbf{x}}'}{\partial \gamma_{\mathbf{i}}}\right)_0 = -v_{\mathbf{s}} \cos (\theta_{\mathbf{s}} - \beta_{\mathbf{s}}) \left(\frac{\partial \theta_{\mathbf{s}}}{\partial \gamma_{\mathbf{i}}}\right)_0 \quad (50)$$

$$\left(\frac{\partial \dot{\mathbf{y}}'}{\partial \gamma_{\mathbf{i}}}\right)_0 = -v_{\mathbf{s}} \sin (\theta_{\mathbf{s}} - \beta_{\mathbf{s}}) \left(\frac{\partial \theta_{\mathbf{s}}}{\partial \gamma_{\mathbf{i}}}\right)_0 \quad (51)$$

where, from equation (43),

$$\left(\frac{\partial \theta_{\mathbf{s}}}{\partial \gamma_{\mathbf{i}}}\right)_0 = \left(\frac{E \frac{\partial D}{\partial \gamma_{\mathbf{i}}} - D \frac{\partial E}{\partial \gamma_{\mathbf{i}}}}{D^2 + E^2}\right)_0 \quad (52)$$

Specifically, if γ is composed of the components of λ_0 and λ_0 , then from equation (43):

$$\frac{\partial D}{\partial \gamma_{\mathbf{1}}} = \left(\frac{\partial D}{\partial \lambda_{\mathbf{1}}}\right)_0 = -v_{\mathbf{s}} \cos \beta_{\mathbf{s}} \quad (53)$$

$$\frac{\partial E}{\partial \gamma_1} = \left(\frac{\partial E}{\partial \lambda_1} \right)_0 = v_s \sin \beta_s \quad (54)$$

$$\frac{\partial D}{\partial \gamma_2} = \left(\frac{\partial D}{\partial \lambda_2} \right)_0 = v_s \sin \beta_s \quad (55)$$

$$\frac{\partial E}{\partial \gamma_2} = \left(\frac{\partial E}{\partial \lambda_2} \right)_0 = v_s \cos \beta_s \quad (56)$$

$$\frac{\partial D}{\partial \gamma_3} = \left(\frac{\partial D}{\partial \kappa_1} \right)_0 = 0 \quad (57)$$

$$\frac{\partial E}{\partial \gamma_3} = \left(\frac{\partial E}{\partial \kappa_1} \right)_0 = r_s \quad (58)$$

$$\frac{\partial D}{\partial \gamma_4} = \left(\frac{\partial D}{\partial \kappa_2} \right)_0 = r_s \quad (59)$$

$$\frac{\partial E}{\partial \gamma_4} = \left(\frac{\partial E}{\partial \kappa_2} \right)_0 = 0 \quad (60)$$

Substituting equations (53) to (60) into equation (52):

$$\left(\frac{\partial \theta_s}{\partial \lambda_1} \right)_0 = - \left[\frac{v_s^2 \lambda_2 + v_s r_s (\kappa_1 \cos \beta_s + \kappa_2 \sin \beta_s)}{D^2 + E^2} \right]_0 \quad (61)$$

$$\left(\frac{\partial \theta_s}{\partial \lambda_2} \right)_0 = \left[\frac{v_s^2 \lambda_1 + v_s r_s (\kappa_1 \sin \beta_s - \kappa_2 \cos \beta_s)}{D^2 + E^2} \right]_0 \quad (62)$$

$$\left(\frac{\partial \theta_s}{\partial \lambda_1}\right)_0 = - \left[\frac{r_s v_s (-\lambda_1 \cos \beta_s + \lambda_2 \sin \beta_s) + r_s^2 \lambda_2}{D^2 + E^2} \right]_0 \quad (63)$$

$$\left(\frac{\partial \theta_s}{\partial \lambda_2}\right)_0 = \left[\frac{r_s v_s (\lambda_1 \sin \beta_s + \lambda_2 \cos \beta_s) + r_s^2 \lambda_1}{D^2 + E^2} \right]_0 \quad (64)$$

Finally, substituting equations (61) to (64) into each of the equations (48) to (51) leads to the sixteen equations that determine the initial values of the analytical partial derivatives $\partial R/\partial \gamma_i$ and $\partial V/\partial \gamma_i$. These equations are not listed here in their completely written out form because of their length and number.

The other partial derivatives have the initial value:

$$\frac{\partial \lambda_i}{\partial \lambda_j} = \frac{\partial \kappa_i}{\partial \kappa_j} = \begin{cases} 1 & \text{if } i = j \\ 0 & \text{if } i \neq j \end{cases} \quad (65)$$

$$\frac{\partial \lambda_i}{\partial \lambda_j} = \frac{\partial \kappa_i}{\partial \lambda_j} = \frac{\partial \sigma}{\partial \lambda_i} = \frac{\partial \sigma}{\partial \kappa_i} = \frac{\partial m}{\partial \lambda_i} = \frac{\partial m}{\partial \kappa_i} = 0 \quad (66)$$

REFERENCES

1. Strack, William C.: Combined High-Low Thrust Propulsion for the Close Solar Probe Mission. NASA TN D-3145, 1965.
2. Horsewood, J. L.: Interplanetary Trajectory Analysis for Combined High- and Low-Thrust Propulsion Systems. American Astronautical Society Space Flight Mechanics Specialists Symposium. Vol. 11 of the AAS Science and Technology Series. M. L. Anthony, ed., American Astronautical Society, 1967, pp. 457-476.
3. Lebedev, V. N.: Variational Problem of Escape from Circular Orbit. Rep. No. FTD-TT-64-1200/1+2+4, Foreign Technology Div., Air Force Systems Command, Dec. 5, 1964. (Available from DDC as AD-610208.)
4. Leitmann, G.: Variational Problems with Bounded Control Variables. Optimization Techniques with Applications to Aerospace Systems. George Leitmann, ed., Academic Press, 1962, Ch. 5.
5. Pines, Samuel: Constants of the Motion for Optimum Thrust Trajectories in a Central Force Field. AIAA J., vol. 2, no. 11, Nov. 1964, pp. 2010-2014.
6. MacKay, John S.; and Rossa, Leonard G.: A Variational Method for the Optimization of Interplanetary Round-Trip Trajectories. NASA TN D-1660, 1963.
7. Breakwell, J. V.: Optimization of Trajectories. General Research in Flight Sciences, January 1959 - January 1960. Vol. III - Flight Dynamics and Space Mechanics. Rep. No. LMSD-288139, Vol. 3, Lockheed Aircraft Corp., 1960, sec. 12.
8. Strack, William C.; and Huff, Vearl N.: The N-Body Code - A General Fortran Code for the Numerical Solution of Space Mechanics Problems on an IBM 7090 Computer. NASA TN D-1730, 1963.
9. Tisserand, Francois Félix: Théories des Satellites de Jupiter et de Saturne Perturbations des Petites Planètes. Traité de Mécanique Céleste, T. 4, Gauthier-Villats (Paris), 1896.
10. Moeckel, W. E.: Trajectories With Constant Tangential Thrust in Central Gravitational Fields. NASA TR R-53, 1959.
11. Melbourne, W. G.: Interplanetary Trajectories and Payload Capabilities of Advanced Propulsion Vehicles. Tech. Rep. 32-68, Jet Propulsion Lab., Calif. Inst. Tech., Mar. 1961.
12. Ting, Lu; and Brofman, Sherwood: On Take-off from Circular Orbit by Small Thrust. Zeit. Angew. Math. Mech., vol. 44, nos. 10-11, Oct.-Nov. 1964, pp. 417-428.

TABLE I. - PROBLEM CONSTANTS

Problem variable	Assumed value
Gravitational constant of Sun, km^3/sec^2	$1.32715445 \times 10^{11}$
Gravitational constant of Earth, km^3/sec^2	3.986032×10^5
Astronomical units (AU), m	1.49599×10^{11}
Earth radius, m	6 378 165
Initial altitude above surface of Earth, km	185
Period of Earth about Sun, days	365.256
Final radius, \bar{r} , m	2.278×10^{11}
Final velocity, \bar{V} , m/sec	24 100
Specific impulse, sec	5000

TABLE II. - SAMPLE CASES FOR TRANSFERS FROM 185-KILOMETER
ALTITUDE PERIGEE AT EARTH TO ORBIT OF MARS

[Angle between Earth at time zero and final rocket position, 225° .]

Case	Total trip time, days	Type of initial orbit Earth	Characteristic velocity increment, ΔV , m/sec	Initial thrust- weight ratio, F/W	Propellant fraction
1	275	Parabolic	8 074	10^{-4}	0.15185
2	275	Circular	15 853	10^{-4}	.27626
3	275	Parabolic	11 318	0.56×10^{-4}	.20613
4	240	Parabolic	20 390	10^{-4}	.34022

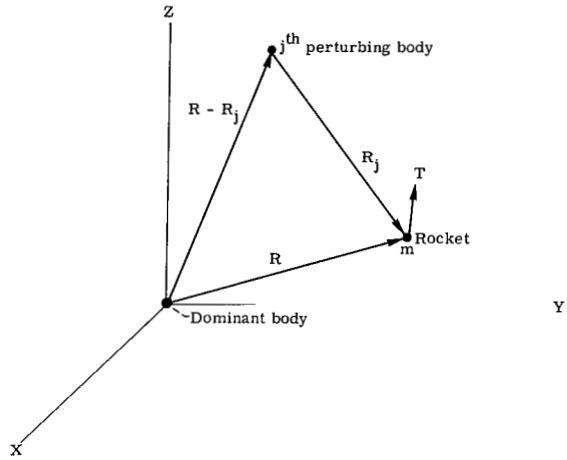


Figure 1. - Coordinate system definition.

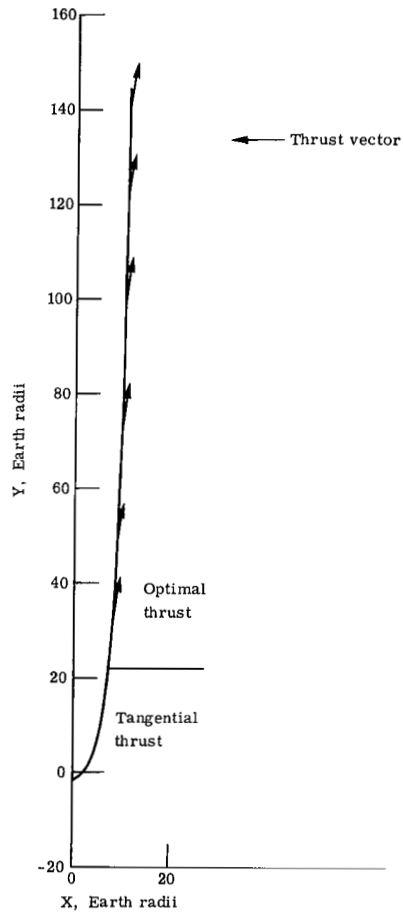


Figure 2. - Earth escape path for three-body solution. Initial Earth orbit, parabolic (case 1); initial thrust-weight ratio, 10^{-4} .

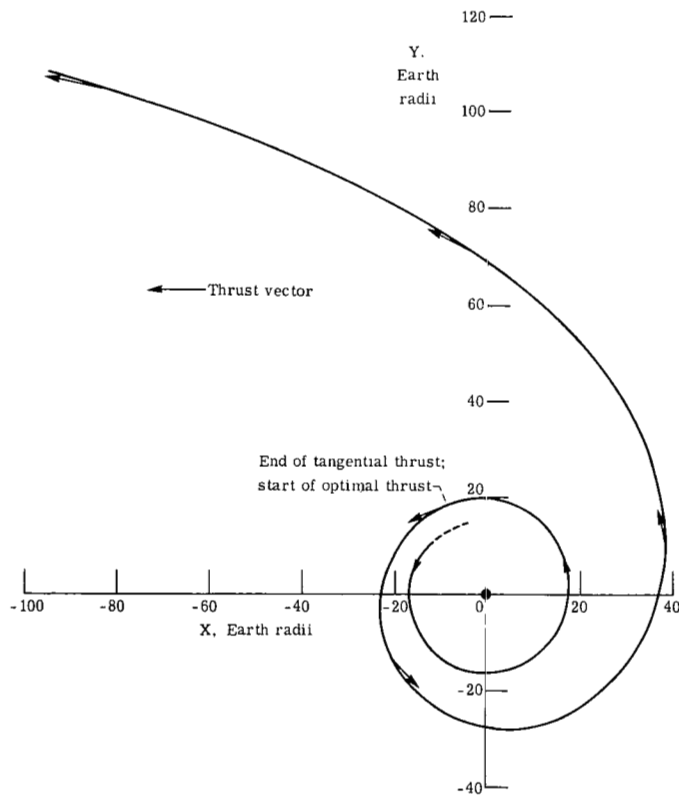
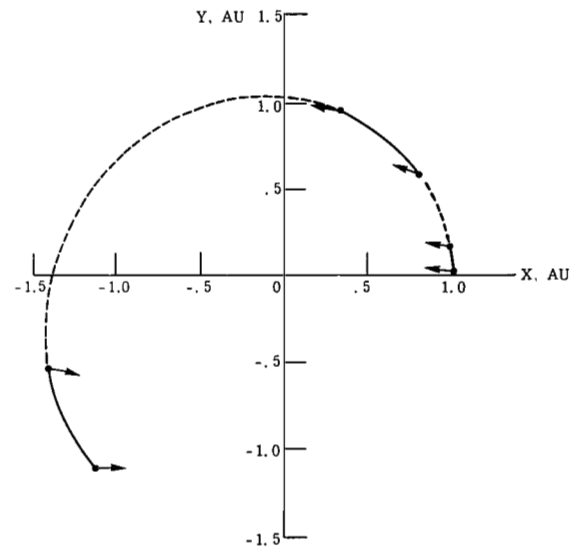
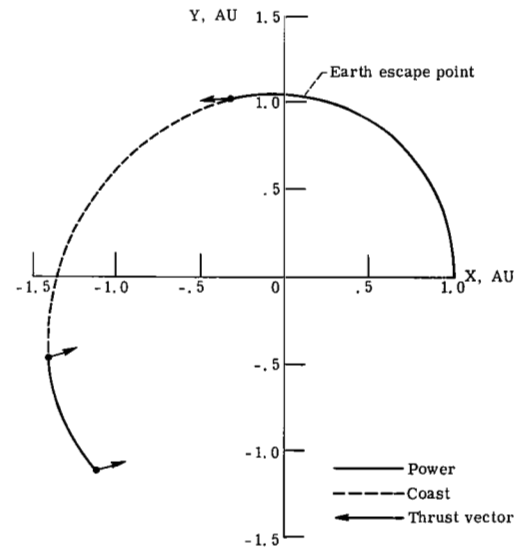


Figure 3. - Earth escape path for three-body solution (last two turns). Initial Earth orbit, circular (case 2); initial thrust-weight ratio, 10^{-4} .



(a) Initial Earth orbit, parabolic (case 1).



(b) Initial Earth orbit, circular (case 2).

Figure 4. - Heliocentric trajectories for three-body solutions. Initial thrust-weight ratio, 10^{-4} .

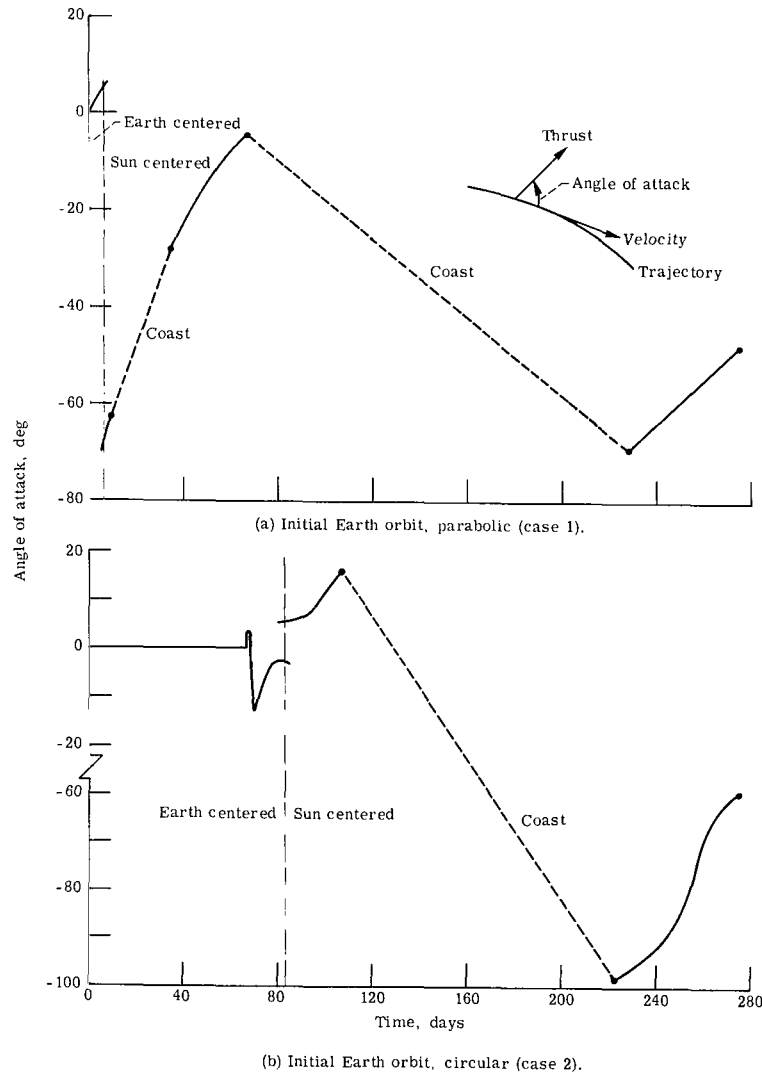


Figure 5. - Thrust angle program for three-body solution. Initial thrust-weight ratio, 10^{-4} .

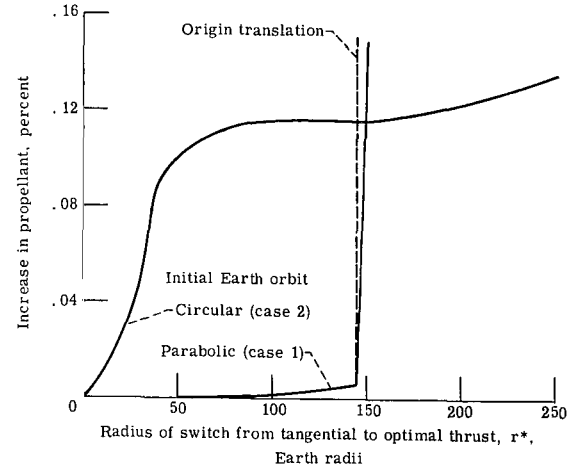


Figure 6. - Effect of using tangential thrust instead of optimal thrust at beginning of flight for three-body solution. Initial thrust-weight ratio, 10^{-4} .

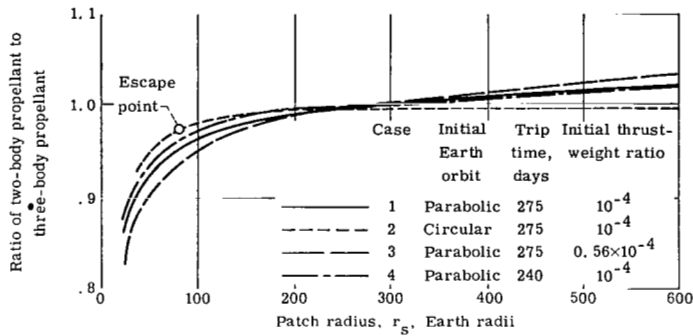


Figure 7. - Propellant comparison between three-body solution and two-body solution with tangential thrust in planetocentric space.

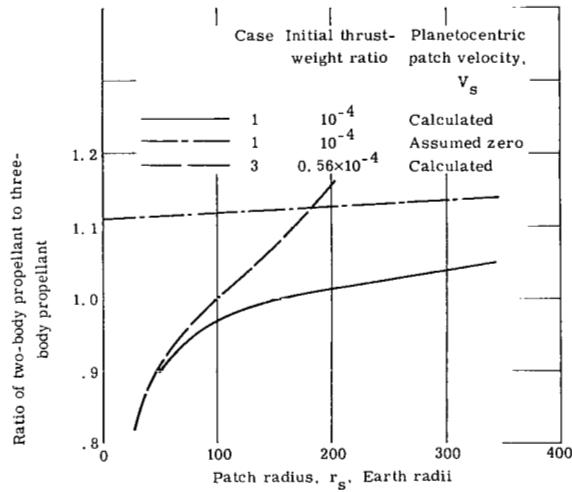


Figure 8. - Propellant comparison between three-body solution and two-body solution with coasting in planetocentric space. Initial Earth orbit, parabolic.

FIRST CLASS MAIL

100-001-55-51-305 68106 00903
AERONAUTICAL ENGINEERING LABORATORY/AFWL
KIRTLAND AIR FORCE BASE, NEW MEXICO 87117

AERONAUTICAL ENGINEERING LABORATORY/AFWL
KIRTLAND AIR FORCE BASE, NEW MEXICO 87117

POSTMASTER: If Undeliverable (Section 158
Postal Manual) Do Not Return

"The aeronautical and space activities of the United States shall be conducted so as to contribute . . . to the expansion of human knowledge of phenomena in the atmosphere and space. The Administration shall provide for the widest practicable and appropriate dissemination of information concerning its activities and the results thereof."

— NATIONAL AERONAUTICS AND SPACE ACT OF 1958

NASA SCIENTIFIC AND TECHNICAL PUBLICATIONS

TECHNICAL REPORTS: Scientific and technical information considered important, complete, and a lasting contribution to existing knowledge.

TECHNICAL NOTES: Information less broad in scope but nevertheless of importance as a contribution to existing knowledge.

TECHNICAL MEMORANDUMS: Information receiving limited distribution because of preliminary data, security classification, or other reasons.

CONTRACTOR REPORTS: Scientific and technical information generated under a NASA contract or grant and considered an important contribution to existing knowledge.

TECHNICAL TRANSLATIONS: Information published in a foreign language considered to merit NASA distribution in English.

SPECIAL PUBLICATIONS: Information derived from or of value to NASA activities. Publications include conference proceedings, monographs, data compilations, handbooks, sourcebooks, and special bibliographies.

TECHNOLOGY UTILIZATION PUBLICATIONS: Information on technology used by NASA that may be of particular interest in commercial and other non-aerospace applications. Publications include Tech Briefs, Technology Utilization Reports and Notes, and Technology Surveys.

Details on the availability of these publications may be obtained from:

SCIENTIFIC AND TECHNICAL INFORMATION DIVISION
NATIONAL AERONAUTICS AND SPACE ADMINISTRATION
Washington, D.C. 20546

